

The Nuclear Stellar Disk in Andromeda: A Fossil from the Era of Black Hole Growth

Philip F. Hopkins^{1*} & Eliot Quataert¹

¹*Department of Astronomy and Theoretical Astrophysics Center, University of California Berkeley, Berkeley, CA 94720*

Submitted to MNRAS, February 2, 2009

ABSTRACT

The physics of angular momentum transport from galactic scales ($\sim 10 - 100$ pc) to much smaller radii is one of the outstanding problems in our understanding of the formation and evolution of super-massive black holes (BHs). Seemingly unrelated observations have discovered that there is a lopsided stellar disk of unknown origin orbiting the BH in M31, and possibly many other systems. We show that these nominally independent puzzles are in fact closely related. Multi-scale simulations of gas inflow from galactic to BH scales show that when sufficient gas is driven towards a BH, gravitational instabilities form a lopsided, eccentric disk that propagates inwards from larger radii. The lopsided stellar disk exerts a strong torque on the remaining gas, driving inflows that fuel the growth of the BH and produce quasar-level luminosities. The same disk can produce significant obscuration along many sightlines and thus may be the putative “torus” invoked to explain obscured active galactic nuclei and the cosmic X-ray background. The stellar relic of this disk is long lived and retains the eccentric pattern. Simulations that yield quasar-level accretion rates produce relic stellar disks with kinematics, eccentric patterns, precession rates, and surface density profiles in reasonable agreement with observations of M31. The observed properties of nuclear stellar disks can thus be used to constrain the formation history of super-massive BHs.

Key words: galaxies: active — quasars: general — galaxies: evolution — cosmology: theory

1 INTRODUCTION

A massive black hole (BH) resides at the center of most massive galaxies (Kormendy & Richstone 1995; Gebhardt et al. 2000; Merritt & Ferrarese 2001). Such BHs gain most of their mass as luminous quasars (Soltan 1982; Yu & Tremaine 2002). A long-standing problem in understanding the origin of massive BHs is how gas loses angular momentum and inflows from galactic scales all the way to the BH. Moreover, the self-gravity of gas can cause it to locally collapse and turn into stars; whatever process drives inflow must compete against gas consumption via star formation. It is now well-established that on relatively large scales within a galaxy, disturbances from collisions with other galaxies and global self-gravitating instabilities can bring the gas down to radii ($\sim 10 - 100$ pc) where the direct gravitational force of the BH begins to dominate the dynamics (Shlosman et al. 1989; Schweizer 1998; Barnes 1998). However, the BH also efficiently suppresses the disturbances from larger scales. How, then, does the gas continue to flow in? On the smallest scales ($\ll 0.1$ pc), accretion can occur through angular momentum transport by local magnetic stresses (Balbus & Hawley 1998). But this leaves a critical gap of a factor

of $\sim 10^{2-3}$ in radius, in which gas is still weakly self-gravitating and can form stars, but both larger-scale torques and local magnetic stresses are inefficient; models have traditionally had great difficulty in crossing this gap (Shlosman & Begelman 1989; Goodman 2003; Thompson et al. 2005).

Independent observations of the properties of stars close to BHs in nearby galaxies have, in some cases, discovered that many of the old stars reside in an eccentric, lopsided stellar disk on spatial scales from $\sim 1 - 10$ pc (Lauer et al. 1996, 2005; Houghton et al. 2006; Thatte et al. 2000; Debattista et al. 2006). The most well-known and well-studied case is in the neighbor to the Milky Way, the Andromeda galaxy, M31 (Lauer et al. 1993; Tremaine 1995; Bender et al. 2005). The dynamics of this disk have received considerable attention, but its origin remains poorly understood (Peiris & Tremaine 2003; Salow & Statler 2004; Bender et al. 2005).

To understand the angular momentum transport required for massive BH growth, we have recently carried out a series of numerical simulations of inflow from galactic to BH scales (Hopkins & Quataert 2009).¹ By re-simulating the central regions of galaxies, gas flows can be followed from galactic scales of ~ 100 kpc to

* E-mail: phopkins@astro.berkeley.edu

¹ Movies of these simulations are available at http://www.cfa.harvard.edu/~phopkins/Site/Movies_zoom.html

much smaller radii, with an ultimate spatial resolution < 0.1 pc. For sufficiently gas-rich disk systems, gas inflow continues all the way to $\lesssim 0.1$ pc. Near the radius of influence of the BH, the systems become unstable to the formation of lopsided, eccentric gas+stellar disks. This eccentric pattern is the dominant mechanism of angular momentum transport at $\lesssim 10$ pc, and can lead to accretion rates as high as $\sim 10 M_\odot \text{ yr}^{-1}$, sufficient to fuel the most luminous quasars. In addition, through this process, some of the gas continuously turns into stars and builds up a nuclear stellar disk. In this *Letter*, we examine the possibility that the nuclear stellar disks seen in M31 and other galaxies are “fossils” from the era of BH growth. If correct, this provides a powerful new set of constraints on the formation and evolution of supermassive BHs.

2 THE SIMULATIONS

Hopkins & Quataert (2009) give a detailed description of the simulations used here; we briefly summarize some of their most important properties. The simulations were performed with the parallel TreeSPH code GADGET-3 (Springel 2005). The simulations include collisionless stellar disks and bulges, dark matter halos, gas, and BHs. For this study, we are interested in isolating the physics of gas inflow. As a result, we do not include models for BH accretion and feedback – the BH’s mass is constant in time and its only dynamical role is via its gravitational influence on scales $\lesssim 10$ pc.

Because of the very large dynamic range in both space and time needed for the self-consistent simulation of galactic inflows and nuclear disk formation, we use a “zoom-in” re-simulation approach. This begins with a large suite of simulations of galaxy-galaxy mergers, and isolated bar-(un)stable disks. These simulations have 0.5×10^6 particles, corresponding to a spatial resolution of 50 pc. These simulations have been described in a series of previous papers (Di Matteo et al. 2005; Robertson et al. 2006; Cox et al. 2006; Younger et al. 2008; Hopkins et al. 2009). From this suite of simulations, we select representative simulations of gas-rich major mergers of Milky-Way mass galaxies (baryonic mass $10^{11} M_\odot$), and their isolated but bar-unstable analogues, to provide the basis for our re-simulations. The dynamics on smaller scales does not depend critically on the details of the larger-scale dynamics. Rather, the small-scale dynamics depends primarily on global parameters of the system, such as the total gas mass channeled to the center relative to the pre-existing bulge mass.

Following gas down to the BH accretion disk requires much higher spatial resolution than is present in the galaxy-scale simulations. We begin by selecting snapshots from the galaxy-scale simulations at key epochs. In each, we isolate the central $0.1 - 1$ kpc region, which contains most of the gas that has been driven in from large scales. Typically this is about $10^{10} M_\odot$ of gas, concentrated in a roughly exponential profile with a scale length of $\sim 0.3 - 0.5$ kpc. From this mass distribution, we then re-populate the gas in the central regions at much higher resolution, and simulate the dynamics for several local dynamical times. These simulations involve 10^6 particles, with a resolution of a few pc and particle masses of $\approx 10^4 M_\odot$. We have run ~ 50 such re-simulations, corresponding to variations in the global system properties, the model of star formation and feedback, and the exact time in the larger-scale dynamics at which the re-simulation occurs. Hopkins & Quataert (2009) present a number of tests of this re-simulation approach and show that it is reasonably robust for this problem. This is largely because, for gas-rich disk systems, the central ~ 300 pc becomes strongly self-gravitating, generating instabilities that dominate the subsequent dynamics.

These initial re-simulations capture the dynamics down to

~ 10 pc, still insufficient to quantitatively describe accretion onto a central BH. We thus repeat our re-simulation process once more, using the central $\sim 10 - 30$ pc of the first re-simulations to initialize a new set of even smaller-scale simulations. These typically have $\sim 10^6$ particles, a spatial resolution of 0.1 pc, and a particle mass $\approx 100 M_\odot$. We carried out ~ 50 such simulations to test the robustness of our conclusions and survey the parameter space of galaxy properties. These final re-simulations are evolved for $\sim 10^7$ years – many dynamical times at 0.1 pc, but very short relative to the dynamical times of the larger-scale parent simulations.²

Our simulations include gas cooling and star formation, with gas forming stars at a rate motivated by the observed Kennicutt (1998) relation. Specifically, we use a star formation rate per unit volume $\dot{\rho}_* \propto \rho^{3/2}$ with the normalization chosen so that a Milky-way like galaxy has a total star formation rate of about $1 M_\odot \text{ yr}^{-1}$. Because we cannot resolve the detailed processes of supernovae explosions, stellar winds, and radiative feedback, feedback from stars is modeled with an effective equation of state (Springel & Hernquist 2003). In this model, feedback is assumed to generate a non-thermal (turbulent, in reality) sound speed that depends on the local star formation rate, and thus the gas density. We use sub-grid sound speeds $\sim 20 - 100 \text{ km s}^{-1}$, motivated by a variety of observations of dense, star forming regions both locally and at high redshift (Downes & Solomon 1998; Bryant & Scoville 1999; Förster Schreiber et al. 2006; Iono et al. 2007). Within this range, we found little difference in the physics of angular momentum transport or in the resulting accretion rates, gas masses, etc. (Hopkins & Quataert 2009) (see also §3).

3 RESULTS

Figure 1 shows an example of the results of our re-simulations. We follow the merger and coalescence of two Milky-way mass galaxies, a highly asymmetric event chosen because it is likely to lead to rapid BH growth. The first image (top left) provides a large-scale view of the system just after the coalescence of the two galactic nuclei and their central BHs. The highly asymmetric disturbances visible in the image (e.g. tidal tails) efficiently torque the gas and allow it to flow inwards. Inside the central $\sim \text{kpc}$, the inflowing gas piles up at the point where its gravity begins to dominate that of the stars and dark matter; this dense gas generates a luminous burst of star formation. Precisely because the gas and newly-formed stars are self-gravitating, they form secondary gravitational instabilities such as bars and spiral waves that produce further torques and inflow. This is essentially the “bars within bars” mechanism proposed in Shlosman et al. (1989) and it occurs for the reasons outlined therein. But once the gas reaches ~ 10 pc, this mechanism no longer works – the gravity of the BH begins to dominate ($M_{\text{BH}} = 3 \times 10^7 M_\odot$ here) and the system can no longer support the large-scale bars critical to the inflow on larger scales.

At precisely these scales our simulations demonstrate that a new instability generically arises – a nearly static (slowly precessing) lopsided or eccentric disk of gas and stars. Such slowly varying eccentric ($m = 1$) perturbations are unique to the gravitational field of a point mass such as a BH (Tremaine 2001). But they are also linearly stable (Tremaine 2001), so how do they arise in the simulations? We discuss this in detail in Hopkins & Quataert (2009); to

² We also carried out a few extremely high-resolution intermediate-scale simulations, which include $\sim 5 \times 10^7$ particles and resolve structure from $\sim \text{kpc}$ to ~ 0.3 pc – these are slightly less high-resolution than the net effect of our two zoom-ins, but they obviate the need for a second zoom-in iteration. The conclusions from these higher resolution simulations are identical.

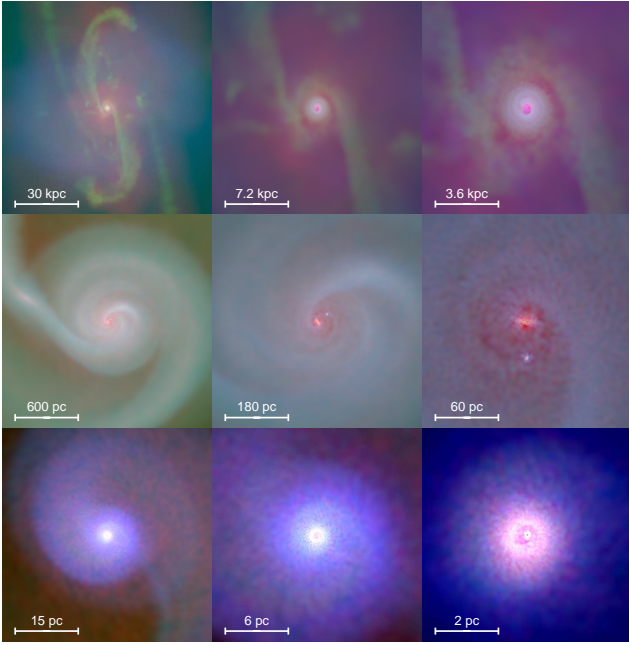


Figure 1. Example of the multi-scale simulations used to follow gas inflow from galactic to nuclear scales. In each panel, red colors denote the projected stellar mass density, and green/blue colors denote the projected gas density (with the variation from green to blue reflecting an increasing star formation rate per unit mass in the gas). Each image is rotated to project the gas density face on, relative to its net angular momentum vector *Top*: Galaxy-scale: the merger of two similar-mass galaxies, just after the final coalescence of the two nuclei (two $10^{11} M_{\odot}$ galaxies with a disk gas fraction $f_{\text{gas}} \sim 0.4$ at the time of merger, and an initial bulge to total mass ratio of $B/T = 0.2$; simulation b3ex(co) in Hopkins & Quataert 2009). The merger has driven large amounts of gas into the central ~ 1 kpc, forming the nuclear starburst shown. *Middle*: Re-simulation of the $\sim 0.1 - 1$ kpc region (simulation If9b5). The starburst disk, being strongly self-gravitating, develops a spiral and bar mode that drives gas to ~ 10 pc, where the bar is suppressed by the gravity of the BH. *Bottom*: Re-simulation of the central ~ 30 pc (simulation Nf8h1c1qs). The inflow to these scales rapidly forms a lopsided eccentric disk around the BH (which maps onto a one-armed spiral at larger radii). The disk drives accretion rates of $\sim 1 - 10 M_{\odot} \text{ yr}^{-1}$ to < 0.1 pc, and leaves the eccentric stellar relics shown in Figures 2 & 3.

summarize, we believe that the mode is a *global* phenomena that grows from the outside in. It first starts to grow because of self-gravity, where the mass of the (stellar + gas) disk is comparable to the mass of the BH. In the simulations, this occurs at $\sim 10 - 100$ pc. Gas moving in circular orbits passes through this eccentric disk, and experiences a torque from the stars therein, causing the gas to lose angular momentum and fall inwards. Some of the gas turns into stars, those stars are excited into the $m = 1$ mode, allowing the perturbation to efficiently propagate inwards to ~ 0.1 pc. Although at radii where $M_{\text{disk}}(< R) \ll M_{\text{BH}}$, the system may formally be stable, the eccentric pattern is *induced* by the mass distribution at somewhat larger radii. The lopsided or eccentric disk, then, is a coherent global pattern superimposed on the otherwise axisymmetric gas and stellar mass distribution. The eccentric pattern precesses with an angular pattern speed Ω_p , which we measure to be $\sim 1 - 5 \text{ km s}^{-1} \text{ pc}^{-1}$ (independent of radius), set by the rotation rate at the radii where the disk and BH masses are comparable.

We have run a suite of over ~ 50 simulations in order to study the properties of, and robustness of, the eccentric disks in our calculations. Figure 2 shows face-on and edge-on views of the gas

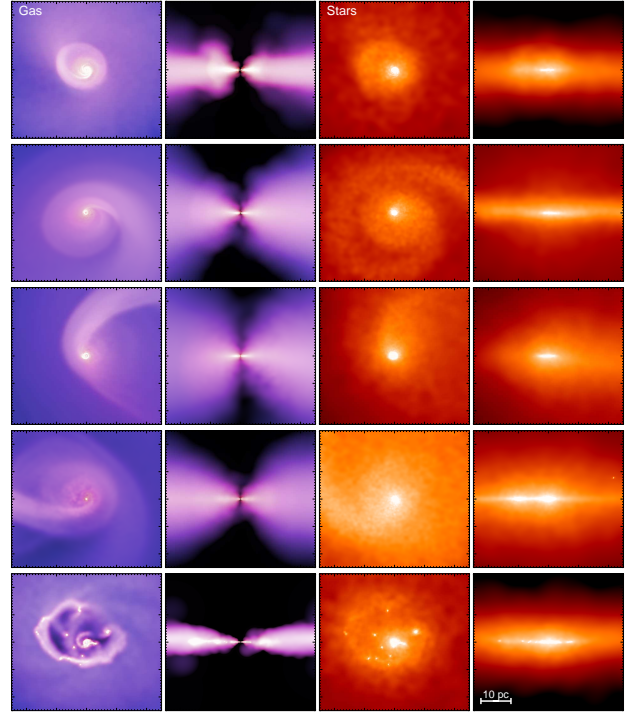


Figure 2. The nuclear disk in several representative simulations. Scale in all panels is the same (lower right). The different rows show the results from simulations of the central ~ 50 pc of galactic nuclei with different galaxy properties (top to bottom: Nf8h1c0thin, Nf8h1c1thin, Nf8h1c1qs, Nf8h1cdens, Nf8h1c0 in Hopkins & Quataert 2009, which have initial $f_{\text{gas}} \sim 0.5 - 0.8$, $h/R = 0.16, 0.08, 0.28, 0.25, 0.15$, $M_{\text{BH}} \sim 3 \times 10^7 M_{\odot}$, and initial disk mass $\sim 1.2, 1.7, 3.0, 8.1, 0.25 \times 10^7 M_{\odot}$ inside 10 pc), and different treatments of stellar feedback (sub-grid sound speeds $c_s \sim 35, 20, 40, 50, 10 \text{ km s}^{-1}$ from top to bottom). The formation of a lopsided disk is ubiquitous. *Left*: Gas surface density. Colors encode the absolute star formation rate of the gas (increasing from blue to red/yellow). Regions where gas shocks (edges in this image) dissipate energy, leading to rapid gas inflow. *Middle Left*: Same, viewed edge-on in cylindrical (R, z) coordinates to emphasize the disk thickness versus radius. The exact thickness depends on our model for stellar feedback, but gravitationally driven turbulence and heating results in the disks always being somewhat flared and thick on these scales, even with negligible stellar feedback (*bottom row*). *Middle Right*: As *left*, but showing the stellar mass distribution. The lack of shocks means that the edges of the disk are less sharp, but they are still visually clear. *Right*: Edge-on stellar density (x, z) . Several of the systems appear to almost have two nuclei, which was the initial indication of the eccentric disk in M31.

and stars in several of these simulations. Provided that a significant amount of gas ($\gtrsim 10\% M_{\text{BH}}$) can be driven in from larger radii by global torques in galaxies, eccentric nuclear disks are generic.

As the flow of gas through the nuclear region subsides, a stellar remnant will remain behind that can retain the eccentric pattern. The characteristic radii $\sim 1 - 10$ pc and stellar masses $\sim 0.1 - 1 M_{\text{BH}}$ of the eccentric nuclear disks in our simulations are reasonably consistent with those observed in M31 and other systems. Figure 2 shows stellar density maps for several of our simulations, including those that have exhausted most of their gas. The distinct nuclear disk is evident. Figure 3 shows the velocity field of the stars in these relics, long after the gas is exhausted, and scaled as if observed at the center of M31; the data for M31 are in the bottom panel. The overall agreement is impressive, particularly given that these simulations are not designed to reproduce the observed fea-

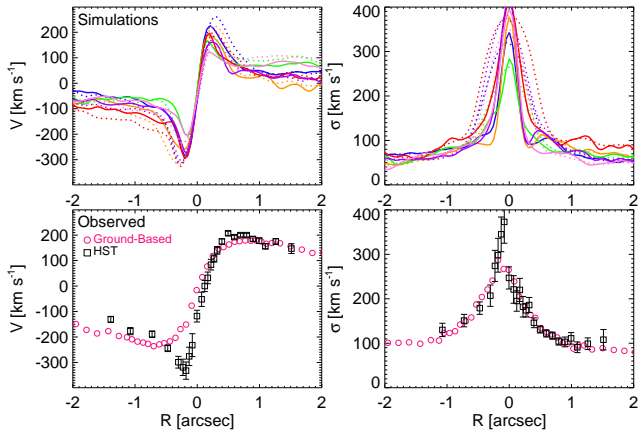


Figure 3. *Top:* Mean projected line-of-sight velocity V (left) and velocity dispersion σ (right) of the relic nuclear stellar disks in our simulations, long after gas is exhausted. Each solid line is a mock line-of-sight velocity field of the stars in one of our simulations, as if they were at the distance and viewing angle of the M31 nucleus (54 deg from edge on; Peiris & Tremaine 2003). Dotted lines vary the inclination angle by 10 deg. The velocities are measured in narrow radial pixels along a slit placed along the major axis. The slit is chosen to match exactly the pixel size, slit width, and resolution limits of the best current observations. *Bottom:* The observations of M31. Our mock profiles are matched to the resolution of the *Hubble Space Telescope* observations shown here (black squares) (Bender et al. 2005). The magenta circles are ground-based observations (Kormendy & Bender 1999) which extend to larger radii but have inferior resolution and smooth the velocity field at $|R| < 1$ arcsec.

tures of M31 in any way, but rather to study the growth of massive BHs. We find similar agreement when comparing to observations of the nuclear disk in NGC 4486b (Lauer et al. 1996).

Figure 4 compares a number of the properties of our simulated relic stellar disks with those of the M31 system inferred from detailed kinematic studies (Salow & Statler 2001; Jacobs & Sellwood 2001; Sambhus & Sridhar 2002; Peiris & Tremaine 2003; Salow & Statler 2004). The range of simulations shown includes both variations in initial conditions and the treatment of stellar feedback (the sub-grid turbulent velocity). Note that the pattern speed Ω_p in our simulations is quite low $\approx 1 - 5 \text{ km s}^{-1} \text{ pc}^{-1}$ (lower left), much less than the rotation rate of individual stars at small radii. In our simulations, the pattern speed is set at the large radii where the eccentric mode begins. The actual precession rate in M31 is not very well-constrained, but most studies place an upper limit of $< 30 \text{ km s}^{-1}$ (Sambhus & Sridhar 2000), and several studies imply a value close to our prediction (see Bacon et al. 2001). The mean disk eccentricity in the simulations is also in broad agreement with that observed, although we find that this is a less robust property of the simulations and varies significantly from one simulation to another.

Figure 4 also shows the inflow rates generated by the nuclear stellar disk during its active/gas-rich phase, as a function of radius. Nuclear disks that are similar to M31 in their relic properties generate accretion rates up to several $M_\odot \text{ yr}^{-1}$ during the quasar epoch, when they are gas-rich. This highlights the key role that eccentric stellar disks can play in fueling the growth of their host BHs.

Our models include a very simplified treatment of the feedback from supernovae and massive stars: we introduce a sub-grid non-thermal sound speed that is a proxy for the effective turbulent speed of the interstellar gas. To test the impact of this on our results, we carried out calculations with identical initial conditions and turbulent velocities ranging from $\sim 10 - 100 \text{ km s}^{-1}$,

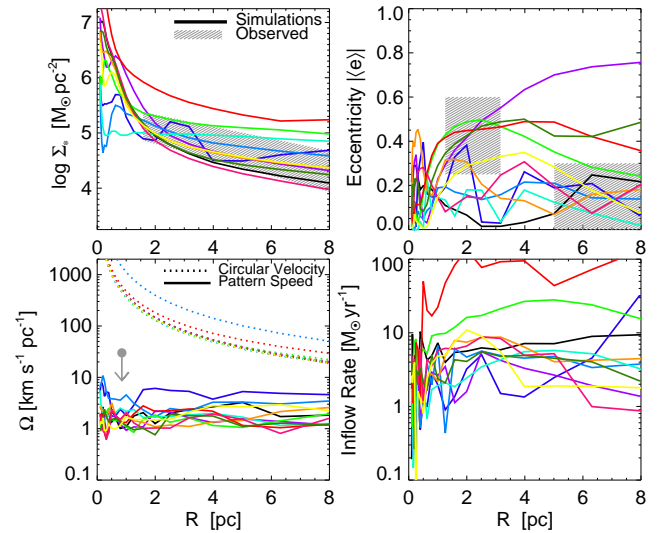


Figure 4. Properties of the simulated nuclear stellar disks versus radii, over the observed scales in M31. Each solid line corresponds to a simulation, as in Figure 3. Where available, we compare with the properties of the M31 system inferred from observations (grey shaded regions). *Top Left:* Stellar mass surface density. *Top Right:* Mean eccentricity of the disk along its major axis. *Bottom Left:* Angular pattern speed (precession rate) of the disk, which is much less than the angular velocity of individual stars in the disk (dotted lines). *Bottom Right:* Inflow rate of gas driven by the gravitational torques of the eccentric disk itself, during the active phase when the disk formed. This accretion can produce most of the BHs growth.

roughly the lower and upper limits allowed by observational constraints for the systems of interest (see Fig. 1 of Hopkins & Quataert 2009 and references therein). The value of the sub-grid sound speed has a significant effect on the amount of resolved sub-structure in the simulation, with more sub-structure present in simulations with lower turbulent velocities. This is not surprising since larger turbulent velocities raise the Jeans mass/length, above which gravity is the dominant force. However, all of the simulations show a similar nuclear lopsided disk. In terms of the properties shown in Figures 3 & 4, the differences produced by changing the sub-grid model are similar to the differences produced by somewhat different galaxy properties. The fundamental reason for the weak dependence on the subgrid model is that the torques in our simulations are primarily determined by gravity, not hydrodynamic forces or viscosity (see Hopkins & Quataert 2009 for a detailed discussion). The primary role of the subgrid feedback model is simply to prevent catastrophic fragmentation of the galactic gas.

4 DISCUSSION

Hopkins & Quataert (2009) argue that the dominant mechanism of angular momentum transport in gas-rich galactic nuclei, from near the BH radius influence ($\sim 10 \text{ pc}$) down to the Keplerian viscous accretion disk ($\ll 0.1 \text{ pc}$), is gravitational torques produced by an eccentric, lopsided disk (an $m = 1$ mode); this asymmetric disk forms in our simulations when the disk mass is at least $\sim 10\%$ of the BH mass. These torques provide the “missing link” connecting the gas reservoir on galactic scales to the small-scale accretion disk near the central BH. In this *Letter* we have shown that the long-lived (“fossil”) stellar relics of these disks are remarkably similar to the eccentric stellar disk observed around the BH in M31. This suggests that the stellar kinematics, morphology, etc. in galactic nuclei can provide new insights into the physics of BH growth.

Emboldened by our success, we can use the observed properties of the M31 disk to infer the accretion it was responsible for. If the M31 disk was at one point gas-rich, the eccentric pattern in the stars would produce strong torques in the gas, leading to an accretion rate of $\dot{M} \sim \Sigma_{\text{gas}} R^2 \Omega |\Phi_1/\Phi_0|$ where Φ_1 and Φ_0 are the asymmetric and axisymmetric terms in the gravitational potential, respectively. For the measured BH mass ($10^8 M_\odot$, Bender et al. 2005) and potential of the eccentric disk (Peiris & Tremaine 2003) this implies an accretion rate of $\sim 1 M_\odot \text{ yr}^{-1}$, close to the Eddington limit of $2.4 M_\odot \text{ yr}^{-1}$. More directly, we find that simulations that yield stellar relics in closest agreement with M31 have typical inflow rates at $R \lesssim 0.1 \text{ pc}$ in their active phases of $\sim 0.3 - 5 M_\odot \text{ yr}^{-1}$ (Fig. 4). These accretion rates imply that the observed stellar disk could have helped the M31 BH gain much of its mass.

During the gas-rich phase, the typical column density of gas for an edge-on line of sight through the disk is $N_H \sim 10^{25-26} \text{ atoms cm}^{-2}$, sufficient to obscure the radiation from the BH even in the X-rays. A combination of our model of stellar feedback and self-consistently calculated gravitational perturbations generate large ‘random’ motions in the gas: the disks are thus thick, with column densities sufficient to block the optical light ($N_H \gtrsim 10^{22} \text{ atoms cm}^{-2}$) out to an angle $\sim 20 - 45 \text{ deg}$ above the plane – in other words, a fraction $\sim 30 - 60\%$ of all sightlines will be obscured by gas and dust in the nuclear disk. More detailed conclusions about this obscuration will require a better understanding of the role of gravitational heating and stellar feedback in this unusual region. Nonetheless, the properties of the obscuring disk we infer are strikingly similar to those invoked for the canonical ‘toroidal obscuring region,’ assumed to reside on small scales and to account for most of the optically obscured AGN population (Antonucci 1993; Urry & Padovani 1995; Lawrence 1991). In the context of our model, the observed ubiquity of the torus suddenly has a dynamical origin: it itself helps drive the accretion.

Understanding the longevity of the eccentric disk in M31 has been as challenging as understanding its origin. The precession rate of the disk is slightly different at different radii – this should lead to phase-mixing that ultimately wipes out the coherent eccentricity of the disk. Indeed, we do see that the eccentric pattern damps away at larger radii; however, the pattern at radii $\sim \text{pc}$, where the M31 disk is observed, persists in our simulations as long as they can be reliably evolved, for 10^8 yrs , which is $\sim 10^4$ dynamical times. Self-gravity is likely to help maintain the pattern even longer, in principle for much longer than the age of the universe (Bacon et al. 2001; Jacobs & Sellwood 2001; Salow & Statler 2004).

Our simulations demonstrate that eccentric stellar and gaseous disks form whenever the mass in the disk component in the central $\sim 10 - 30 \text{ pc}$ is comparable to that of the BH (Hopkins & Quataert 2009). It is unclear, however, under what conditions these nuclear stellar disks will survive to the present day. This is key question for future research. Observationally, there are a number of candidate systems in addition to M31, as evidenced by apparently offset centers, ‘hollow’ central light profiles, double nuclei, or chemically distinct secondary nuclei (Lauer et al. 2002, 2005; Debattista et al. 2006; Thatte et al. 2000; Afanasiev & Sil’chenko 2002); and there are other confirmed eccentric disks as well, such as NGC4486b (Lauer et al. 1996).

When nuclear eccentric disks do survive, our models imply that there should be a correspondence between the properties of the nuclear stellar disk (mass, radius, and asymmetry) and the central BH mass, as we have demonstrated is the case in M31. Very low pattern speeds $< 10 \text{ km s}^{-1} \text{ pc}^{-1}$ should be ubiquitous, as they are required for efficient exchange of angular momentum between the

stars and gas. It is also worth noting that if some gas flows in from larger radii, or accumulates via stellar evolution, the nuclear regions can experience recurrent low-level AGN activity and/or star formation, regulated by the same mechanism of eccentric stellar torques (e.g., M31’s young stellar population; Chang et al. 2007). Such episodes may complicate dating the formation epochs of these disks, but also provide a laboratory to study the physics of inflow in detail. The properties of the nuclear disk in its gas-rich phase determines the distribution of implied torus scale lengths and gas densities, which can be probed by infrared adaptive optics observations of nearby bright AGN (Davies et al. 2007; Hicks et al. 2009). On the theoretical side, further improvements in the treatment of gas physics and star formation will enable more detailed comparison with observations.

ACKNOWLEDGMENTS

We thank Phil Chang, Lars Hernquist, Scott Tremaine, John Kormendy, and Tod Lauer for helpful discussions during the development of this work. Support for PFH and EQ was provided by the Miller Institute for Basic Research in Science, University of California Berkeley. EQ was also supported in part by NASA grant NNG06GI68G and the David and Lucile Packard Foundation.

REFERENCES

- Afanasiev, V. L., & Sil’chenko, O. K. 2002, *A&A*, 388, 461
- Antonucci, R. 1993, *ARA&A*, 31, 473
- Bacon, R., Emsellem, E., Combes, F., Copin, Y., Monnet, G., & Martin, P. 2001, *A&A*, 371, 409
- Balbus, S. A., & Hawley, J. F. 1998, *Reviews of Modern Physics*, 70, 1
- Barnes, J. E. 1998, in *Saas-Fee Advanced Course 26: Galaxies: Interactions and Induced Star Formation*; Springer-Verlag Berlin/Heidelberg, ed. R. C. Kennicutt, Jr., F. Schweizer, J. E. Barnes, D. Friedli, L. Martinet, & D. Pfenniger, 275–+
- Bender, R., et al. 2005, *ApJ*, 631, 280
- Bryant, P. M., & Scoville, N. Z. 1999, *AJ*, 117, 2632
- Chang, P., Murray-Clay, R., Chiang, E., & Quataert, E. 2007, *The Astrophysical Journal*, 668, 236
- Cox, T. J., Dutta, S. N., Di Matteo, T., Hernquist, L., Hopkins, P. F., Robertson, B., & Springel, V. 2006, *ApJ*, 650, 791
- Davies, R. I., Sánchez, F. M., Genzel, R., Tacconi, L. J., Hicks, E. K. S., Friedrich, S., & Sternberg, A. 2007, *ApJ*, 671, 1388
- Debattista, V. P., Ferreras, I., Pasquali, A., Seth, A., De Rijcke, S., & Morelli, L. 2006, *ApJL*, 651, L97
- Di Matteo, T., Springel, V., & Hernquist, L. 2005, *Nature*, 433, 604
- Downes, D., & Solomon, P. M. 1998, *ApJ*, 507, 615
- Förster Schreiber, N. M., et al. 2006, *ApJ*, 645, 1062
- Gebhardt, K., et al. 2000, *ApJL*, 539, L13
- Goodman, J. 2003, *MNRAS*, 339, 937
- Hicks, E. K. S., Davies, R. I., Malkan, M. A., Genzel, R., Tacconi, L. J., Sánchez, F. M., & Sternberg, A. 2009, *ApJ*, 696, 448
- Hopkins, P. F., Cox, T. J., Younger, J. D., & Hernquist, L. 2009, *ApJ*, 691, 1168
- Hopkins, P. F., & Quataert, E. 2009, *MNRAS*, in press, arXiv:0912.3257
- Houghton, R. C. W., Magorrian, J., Sarzi, M., Thatte, N., Davies, R. L., & Krajnović, D. 2006, *MNRAS*, 367, 2
- Iono, D., et al. 2007, *ApJ*, 659, 283
- Jacobs, V., & Sellwood, J. A. 2001, *ApJL*, 555, L25
- Kennicutt, Jr., R. C. 1998, *ApJ*, 498, 541

- Kormendy, J., & Bender, R. 1999, *ApJ*, 522, 772
- Kormendy, J., & Richstone, D. 1995, *ARA&A*, 33, 581
- Lauer, T. R., Gebhardt, K., Richstone, D., Tremaine, S., Bender, R., Bower, G., Dressler, A., Faber, S. M., Filippenko, A. V., Green, R., Grillmair, C. J., Ho, L. C., Kormendy, J., Magorrian, J., Pinkney, J., Laine, S., Postman, M., & van der Marel, R. P. 2002, *AJ*, 124, 1975
- Lauer, T. R., et al. 1993, *AJ*, 106, 1436
- . 1996, *ApJL*, 471, L79+
- . 2005, *AJ*, 129, 2138
- Lawrence, A. 1991, *MNRAS*, 252, 586
- Merritt, D., & Ferrarese, L. 2001, *ApJ*, 547, 140
- Peiris, H. V., & Tremaine, S. 2003, *ApJ*, 599, 237
- Robertson, B., Hernquist, L., Cox, T. J., Di Matteo, T., Hopkins, P. F., Martini, P., & Springel, V. 2006, *ApJ*, 641, 90
- Salow, R. M., & Statler, T. S. 2001, *ApJL*, 551, L49
- . 2004, *ApJ*, 611, 245
- Sambhus, N., & Sridhar, S. 2000, *ApJL*, 539, L17
- . 2002, *A&A*, 388, 766
- Schweizer, F. 1998, in *Saas-Fee Advanced Course 26: Galaxies: Interactions and Induced Star Formation* (Springer-Verlag Berlin/Heidelberg), ed. R. C. Kennicutt, Jr., F. Schweizer, J. E. Barnes, D. Friedli, L. Martinet, & D. Pfenniger, 105–+
- Shlosman, I., & Begelman, M. C. 1989, *ApJ*, 341, 685
- Shlosman, I., Frank, J., & Begelman, M. C. 1989, *Nature*, 338, 45
- Soltan, A. 1982, *MNRAS*, 200, 115
- Springel, V. 2005, *MNRAS*, 364, 1105
- Springel, V., & Hernquist, L. 2003, *MNRAS*, 339, 289
- Thatte, N., Tecza, M., & Genzel, R. 2000, *A&A*, 364, L47
- Thompson, T. A., Quataert, E., & Murray, N. 2005, *ApJ*, 630, 167
- Tremaine, S. 1995, *AJ*, 110, 628
- . 2001, *AJ*, 121, 1776
- Urry, C. M., & Padovani, P. 1995, *PASP*, 107, 803
- Younger, J. D., Hopkins, P. F., Cox, T. J., & Hernquist, L. 2008, *ApJ*, 686, 815
- Yu, Q., & Tremaine, S. 2002, *MNRAS*, 335, 965